A&A 490, 613–623 (2008)
DOI: 10.1051/0004-6361:200810192

Astronomy & Astrophysics

Galactic abundance gradients from Cepheids

On the iron abundance gradient around 10–12 kpc

B. Lemasle[1,2], P. François[2], A. Piersimoni[3], S. Pedicelli[4,5], G. Bono[4,5], C. D. Laney[6], F. Primas[4], and M. Romaniello[4,⋆]

[1] Université de Picardie – Jules Verne, Faculté des Sciences, 33 rue Saint-Leu, 80039 Amiens Cedex 1, France
e-mail: bertrand.lemasle@etud.u-picardie.fr
[2] Observatoire de Paris, GEPI, 61 avenue de l'Observatoire, 75014 Paris, France
[3] Istituto Nazionale di Astrofisica, Osservatorio Astronomico di Collurania, via M. Maggini, 64100 Teramo, Italy
[4] European Southern Observatory (ESO), Karl Schwarzschild-Strasse 2, 85748 Garching bei Muenchen, Germany
[5] Istituto Nazionale di Astrofisica, Osservatorio Astronomico di Roma, via Frascati 33, 00040 Monte Porzio Catone, Italy
[6] South African Astronomical Observatory, PO Box 9, 7935 Observatory, South Africa

Received 14 May 2008 / Accepted 5 August 2008

ABSTRACT

Context. Classical Cepheids are excellent tracers of intermediate-mass stars, since their distances can be estimated with very high accuracy. In particular, they can be adopted to trace the chemical evolution of the Galactic disk.
Aims. Homogeneous iron abundance measurements for 33 Galactic Cepheids located in the outer disk together with accurate distance determinations based on near-infrared photometry are adopted to constrain the Galactic iron gradient beyond 10 kpc.
Methods. Iron abundances were determined using high resolution Cepheid spectra collected with three different observational instruments: ESPaDOnS@CFHT, Narval@TBL and FEROS@2.2m ESO/MPG telescope. Cepheid distances were estimated using near-infrared (J, H, K-band) period-luminosity relations and data from SAAO and the 2MASS catalog.
Results. The least squares solution over the entire data set indicates that the iron gradient in the Galactic disk presents a slope of –0.052 ± 0.003 dex kpc^{-1} in the 5–17 kpc range. However, the change of the iron abundance across the disk seems to be better described by a linear regime inside the solar circle and a flattening of the gradient toward the outer disk (beyond 10 kpc). In the latter region the iron gradient presents a shallower slope, i.e. –0.012 ± 0.014 dex kpc^{-1}. In the outer disk (10–12 kpc) we also found that Cepheids present an increase in the spread in iron abundance. Current evidence indicates that the spread in metallicity depends on the Galactocentric longitude. Finally, current data do not support the hypothesis of a discontinuity in the iron gradient at Galactocentric distances of 10–12 kpc.
Conclusions. The occurrence of a spread in iron abundance as a function of the Galactocentric longitude indicates that linear radial gradients should be cautiously treated to constrain the chemical evolution across the disk.

Key words. stars: abundances – stars: supergiants – Galaxy: abundances – Galaxy: evolution – Cepheids

1. Introduction

Chemodynamical evolutionary models provide interesting predictions concerning the formation and evolution of the Milky Way. However, the plausibility and accuracy of these predictions need to be validated with observational data. The most commonly adopted observables are the star formation rate and the abundance gradients across the Galactic disk.

Different tracers have been used to determine the Galactic gradients: HII regions, Open Clusters, O/B-type stars and Cepheids. Compared to other tracers, Cepheids present several advantages: i) they are well-known primary distance indicators; ii) they are bright enough to allow the study of the gradient over a large range of Galactocentric distances; iii) they present a large set of well defined absorption lines, therefore, accurate abundances of many elements can be provided.

Abundance gradients were discovered first by Searle (1971) in six external galaxies using HII regions. However, their occurrence in our Galaxy remained controversial as they are not easy to observe due to the fact we are embedded in the Galactic disk. Indeed, some studies were in favor of Galactic gradients, like D'Odorico et al. (1976) or Janes (1979) whereas others found no correlation between distance and metallicity (Clegg & Bell 1973; Jennens & Helfer 1975). Today, the existence of Galactic abundance gradients seems widely accepted, even if some recent studies still report no evidence of such gradients, but the empirical determinations of their shapes and slopes are strongly debated.

Considering a simple linear gradient the slopes for different elements can be explored with several stellar tracers. The reader interested in exhaustive reviews concerning Galactic gradients is referred to Andrievsky et al. (2002a) and Chiappini et al. (2001). By using HII regions, Vilchez & Esteban (1996) found a slope of –0.02 dex kpc^{-1}, but other authors using the same tracers suggested slopes ranging from –0.039 dex kpc^{-1} (Deharveng et al. 2000) to –0.065 dex kpc^{-1} (Afflerbach et al. 1997). On the other hand, the use of B-type stars gives slopes ranging from –0.042 dex kpc^{-1} (Daflon et al. 2004) to –0.07 dex kpc^{-1}

⋆ Based on observations obtained at the Canada-France-Hawaii Telescope (CFHT) which is operated by the National Research Council of Canada, the Institut National des Sciences de l'Univers of the Centre National de la Recherche Scientifique of France, and the University of Hawaii. Based on observations collected with FEROS at the European Southern Observatory (La Silla, Chile). Based on observations obtained at the Telescope Bernard Lyot (USR5026) operated by the Observatoire Midi-Pyrénées and the Institut National des Science de l'Univers of the Centre National de la Recherche Scientifique of France.

(Gummersbach et al. 1998). The slopes based on planetary nebulae range from –0.05 dex kpc^{-1} (Costa et al. 2004) to –0.06 dex kpc^{-1} (Maciel et al. 1999) to the lack of a Galactic metallicity gradient (Stanghellini et al. 2006). The slopes based on old Open Clusters still show a large spread. By adopting a sample of 40 clusters distributed between the solar circle and $R_G \simeq 14$ kpc, Friel et al. (2002) found a slope of –0.06 dex kpc^{-1}. More recently, Carraro et al. (2007) using new accurate metal abundances for five old open clusters located in the outer disk together with the sample adopted by Friel et al. (2002) found a much shallower global iron gradient, namely –0.018 dex kpc^{-1}. The global iron slopes based on Cepheids are very homogeneous, dating back to the first estimates by Harris (1981, 1984), who found a slope of –0.07 dex kpc^{-1}; the more recent estimates provide slopes ranging from –0.06 dex kpc^{-1} (Andrievsky et al. 2002c; Luck et al. 2003; Andrievsky et al. 2004; Luck et al. 2006) to –0.07 dex kpc^{-1} (Lemasle et al. 2007), hereafter Paper I.

As far as the shape of the gradient is concerned, current findings are even more controversial. In particular, the hypothesis of a linear gradient is still widely debated. Several investigations based on different stellar tracers – HII regions, Vilchez & Esteban (1996), open clusters, Twarog et al. (1997), Carraro et al. (2007), Cepheids, Andrievsky et al. (2004); planetary nebulae, Costa et al. (2004) – indicate a flattening of the Galactic gradient beyond 10–12 kpc. This flattening is well reproduced by chemodynamical evolutionary models (Cescutti et al. 2007). More recently, Yong et al. (2006) brought forward a new feature: the flattening may occur with two different basement values, the first one at –0.5 dex, a value more metal-poor than previous studies, and the second one at –0.8 dex. According to the quoted authors, the latter one might imply the possibility of a merger event. On the other hand, independent studies do not show evidence of a flattening toward the outer disk, like Rolleston et al. (2000) based on O/B stars or Deharveng et al. (2000) based on HII regions. Moreover, a discontinuity in the metallicity gradient at $R_G \sim$ 10–12 kpc has also been suggested by Twarog et al. (1997) according to open cluster photometry. Instead of a regular decrease from the inner to the outer disk, they indicate a 2 zone distribution with an abrupt discontinuity of ∼–0.2 dex at about 10–12 kpc and a shallower gradient inside each zone. This hypothesis was supported by Andrievsky et al. (2002c), Luck et al. (2003) and by Andrievsky et al. (2004). Such variety may be due to the fact that the different tracers adopted to estimate the gradient present only a handful of objects toward the outer disk, i.e. at $R_G \geq 12$ kpc.

In this paper, we investigate the shape of the gradient in the outer disk and focus our attention on the transition zone around 10–12 kpc. The paper is organized as follows: in Sect. 2 we describe the data and the reduction strategy adopted to estimate the iron abundances and the distances. In this section we also discuss the uncertainties affecting both abundances and distances. In Sect. 3 we discuss the new iron abundances and compare them with previous measurements. In Sect. 4, we present the new Galactic iron gradients and compare them with previous estimates based on different stellar tracers. Section 5 summarizes current findings.

2. Observations and data reduction

2.1. Observations

High resolution spectroscopic observations were performed in 2006 with ESPaDOnS at the CFHT (27 stars) and in 2007 with FEROS (Kaufer et al. 1999) at the 2.2 m ESO/MPG telescope in La Silla (6 stars). Another target (BK Aur) already included in the ESPaDOnS sample was also observed in 2007 with Narval at the 2 m Telescope Bernard Lyot (TBL) in Pic du Midi in Southwest France. ESPaDOnS has a resolving power of 81 000 in the spectroscopic "star-only" mode (only the light from the star goes through the instrument) and an has accessible wavelength range of 370–1050 nm. FEROS has a resolving power of 48 000 and an accessible wavelength range of 370–920 nm, while Narval is a copy of ESPaDOnS adapted to the specifics of the TBL, whose resolving power is 75 000 in the spectroscopic "star-only" mode and an accessible wavelength range of 370–1050 nm. The spectra were reduced either using the FEROS package within MIDAS or using the Libre-ESpRIT software (Donati et al. 1997, 2006). Relevant information concerning the observations and the signal-to-noise (*S/N*) ratio at 600 nm are listed in Table 1. Phases were calculated with periods and epochs from the GCVS (General Catalogue of Variable Stars) described in Samus et al. (2004), except for 8 stars to take into account changes in the period. In the case of AO Aur, RZ Gem, SV Mon, UY Mon, RS Ori, GQ Ori, they are from Berdnikov & Ignatova (2000) while in the case of AD Gem and CV Mon they are from Szabados (1991).

2.2. Line list

We started from the iron line list provided by Romaniello et al. (2008) and used in Paper I. This list was extended by following the method devised by the quoted authors to match the wider spectral range of ESPaDOnS and Narval. The atomic properties (oscillator strength, excitation potential) listed in VALD (Vienna Atomic Lines Database) were adopted for all the selected lines.

2.3. Equivalent widths

Measurements of equivalent widths (*EW*) are made with a semi-interactive code based on genetic algorithms from Charbonneau (1995) (see Paper I for details). The analysis takes into account only weak, non blended lines so that all of them can be fitted by a Gaussian. While strong lines are systematically discarded, weak and asymmetric lines are removed after visual inspection. No peculiar treatment was applied to weakly asymmetric lines, like the one proposed by Andrievsky et al. (2005). To ensure the reliability of our *EW*s, we compared them to *EW*s obtained by direct integration of the lines in the case of RZ Gem. As no systematics were found between direct integration and Gaussian fit, we assumed the asymmetry was weak enough so that the lines could still be fitted by Gaussians. The number of lines finally used is on average 80–130 lines for Fe I and 15–25 lines for Fe II.

2.4. Effective temperature estimates

The determination of an accurate temperature is a key point in the abundance determination. Following the same approach adopted in Paper I, the stellar effective temperatures, $T_{\rm eff}$, were estimated using the method of line depth ratios described in Kovtyukh & Gorlova (2000). This approach has the additional advantage of being independent of interstellar reddening. Kovtyukh & Gorlova (2000) proposed 32 analytical relations to derive $T_{\rm eff}$ from line depth ratios. After measuring the line depths and calculating associated ratios, we obtained 32 temperatures whose mean value gave us the stellar temperatures

Table 1. Observations: date, phase, spectrograph, exposure time and *S/N* ratio at 600 nm.

Object	Date	Julian date d	Phase	Spectrograph	Exp. time s	*S/N* (600 nm)
AO Aur	14/02/06	2453781.910	0.632	ESPaDOnS	1500	89
AX Aur	16/02/06	2453783.775	0.619	ESPaDOnS	2*2700	113
BK Aur	14/02/06	2453781.974	0.150	ESPaDOnS	700	101
	31/10/07	2454405.736	0.096	NARVAL	1800	101
SY Aur	15/02/06	2453782.928	0.809	ESPaDOnS	500	125
Y Aur	16/02/06	2453783.911	0.983	ESPaDOnS	800	142
YZ Aur	15/02/06	2453782.712	0.789	ESPaDOnS	1600	145
AO CMa	31/03/07	2454191.099	0.241	FEROS	2700	107
AA Gem	15/02/06	2453782.818	0.749	ESPaDOnS	900	128
AD Gem	15/02/06	2453782.971	0.131	ESPaDOnS	900	126
RZ Gem	15/02/06	2453782.804	0.768	ESPaDOnS	800	91
BE Mon	15/02/06	2453782.886	0.409	ESPaDOnS	1600	120
BV Mon	16/02/06	2453783.950	0.851	ESPaDOnS	1800	79
CV Mon	16/02/06	2453783.928	0.084	ESPaDOnS	1500	152
EK Mon	15/02/06	2453782.838	0.809	ESPaDOnS	1800	103
SV Mon	15/02/06	2453782.955	0.663	ESPaDOnS	300	119
TW Mon	31/03/07	2454191.074	0.664	FEROS	2*1800	80
TX Mon	14/02/06	2453781.932	0.998	ESPaDOnS	1700	111
TY Mon	15/02/06	2453782.737	0.537	ESPaDOnS	1800	72
TZ Mon	14/02/06	2453781.889	0.896	ESPaDOnS	1400	106
UY Mon	16/02/06	2453783.967	0.065	ESPaDOnS	600	107
V495 Mon	15/02/06	2453782.911	0.074	ESPaDOnS	1800	46
V508 Mon	14/02/06	2453781.954	0.101	ESPaDOnS	1700	130
V510 Mon	31/03/07	2454191.029	0.975	FEROS	2*1800	98
WW Mon	16/02/06	2453783.844	0.884	ESPaDOnS	2*2700	104
XX Mon	15/02/06	2453782.863	0.584	ESPaDOnS	1800	58
CS Ori	15/02/06	2453782.761	0.637	ESPaDOnS	1800	78
GQ Ori	15/02/06	2453782.961	0.836	ESPaDOnS	300	125
RS Ori	15/02/06	2453782.981	0.709	ESPaDOnS	350	118
HW Pup	29/03/07	2454189.081	0.906	FEROS	4*1800	93
AV Tau	16/02/06	2453783.722	0.701	ESPaDOnS	2*1800	73
ST Tau	15/02/06	2453782.949	0.696	ESPaDOnS	300	120
DD Vel	26/03/07	2454186.590	0.329	FEROS	4*1800	127
EZ Vel	26/03/07	2454186.495	0.106	FEROS	4*1800	155
	30/03/07	2454190.204	0.214	FEROS	2*1800	129

listed in Table 2. Recently Kovtyukh (2007) increased to 131 the set of relations for the determination of supergiant temperature. We double-checked our temperatures using these new relations (Kovtyukh, private communication) and we found a very good agreement between the two independent estimates.

2.5. Atmospheric parameters

The surface gravity, $\log g$, and the micro-turbulent velocity, v_t, were determined by imposing an ionization balance between Fe I and Fe II with the help of the curve of growth. Lines of the same element in different ionization states should give the same abundance value. Iterations on $\log g$ and v_t are, therefore, repeated until Fe I and Fe II adjust to the same curve of growth. This tool also provides an independent check for the $T_{\rm eff}$ value, since both high and low $\chi_{\rm ex}$ values properly fit the curve of growth. Once abundances were measured, atmospheric parameters are validated by checking that the Fe I abundances depend neither on line strength nor on the excitation potential. The atmospheric parameters for the Cepheids in our sample are listed in Table 2.

2.6. Abundance determinations

Atmospheric parameters are then used as input for stellar atmosphere models. We used the MARCS models of Edvardsson et al. (1993) which are based on the following assumptions: plane-parallel stratification, hydrostatic equilibrium and LTE. The abundance determination codes adjust abundances until a good match between predicted and observed equivalent widths is obtained. The final abundance of a star is estimated as the mean value of the abundances determined for each line. The high *S/N* ratio of the spectra and the use of a substantial number of clean lines provide the opportunity to reduce the intrinsic errors on iron abundance to ~0.12 dex. Note that in this investigation, we adopted the solar chemical abundances provided by Grevesse et al. (1996).

2.7. Uncertainties in abundance determination

The very first source of errors in abundance determination comes from the extraction of data from the spectra. The equivalent width (EW) and the continuum placement must be accurately measured. Thus, we limited our analysis to symmetric and unblended lines, avoiding the most crowded parts of the spectra. We retained only relatively weak lines ($EW \leq 120$ mÅ) for the abundance calculation and checked that they could be fitted by a Gaussian.

The crucial point in the abundance determination is to obtain an accurate temperature as it strongly affects the line strength. As mentioned above, we used the method of line depth ratios from

Table 2. Atmospheric parameters adopted to compute iron abundances.

Object	phase	$T_{\rm eff}$ K	$\log g$ dex	$V_{\rm t}$ km s^{-1}	[Fe/H] dex
AO Aur	0,632	5450	0.8	3.0	–0.41
AX Aur	0.619	5635	0.8	2.7	–0.22
BK Aur	0.150	5970	1.3	3.0	–0.10
	0.096	6160	1.4	3.4	–0.04
SY Aur	0.809	6220	1.1	3.0	–0.07
Y Aur	0.983	6300	1.5	3.0	–0.26
YZ Aur	0.789	5715	1.0	3.5	–0.33
AO CMa	0.241	6065	1.7	3.7	–0.04
AA Gem	0.749	5500	1.0	4.7	–0.35
AD Gem	0.131	6130	1.6	3.0	–0.19
RZ Gem	0.768	5500	0.8	3.3	–0.44
BE Mon	0.409	5865	1.4	3.0	–0.07
BV Mon	0.851	6080	1.9	3.2	–0.10
CV Mon	0.084	6350	2.0	3.1	–0.10
EK Mon	0.809	5700	1.3	3.4	–0.05
SV Mon	0.663	4900	0.5	3.4	–0.10
TW Mon	0.664	5640	1.3	3.4	–0.15
TX Mon	0.998	5945	1.0	3.0	–0.12
TY Mon	0.537	5555	1.2	3.0	–0.15
TZ Mon	0.896	6020	1.3	3.0	–0.04
UY Mon	0.065	6100	1.5	3.0	–0.33
V495 Mon	0.074	6090	1.6	3.2	–0.17
V508 Mon	0.101	6100	1.5	3.2	–0.25
V510 Mon	0.975	5390	0.8	3.3	–0.12
WW Mon	0.884	6650	1.4	3.0	–0.32
XX Mon	0.584	5520	0.9	3.0	–0.18
CS Ori	0.637	6350	2.0	3.1	–0.19
GQ Ori	0.836	4960	2.6	0.8	0.11
RS Ori	0.709	5475	1.3	3.0	–0.14
HW Pup	0.906	5300	0.6	3.1	–0.28
AV Tau	0.701	5750	1.3	3.0	–0.17
ST Tau	0.696	5700	1.4	3.2	–0.14
DD Vel	0.329	5600	1.1	3.2	–0.35
EZ Vel	0.106	6380	1.5	3.6	–0.01
	0.214	5455	0.6	3.6	–0.01

Kovtyukh & Gorlova (2000), according to which the uncertainties on absolute temperatures are at most ≈80 K. Moreover, the curves of growth provided an independent check of the temperature determination as lines with high and low $\chi_{\rm ex}$ values must both fit well the curve of growth. This ensures us that our intrinsic dispersion in temperature is not more than 100 K.

In order to test how the uncertainties affect the final abundance result, we computed abundances by adopting over or under-estimated values of the atmospheric parameters. As expected, only the errors on temperature have a noticeable effect: over or under-estimating the effective temperature of 100 K implies a difference of about ±0.1 dex in the abundance determination. Errors on the surface gravity of $\Delta \log g = \pm 0.3$ dex and on the micro-turbulent velocity of $\Delta v_{\rm t} = \pm 0.5$ km s^{-1} have modest effects as the differences are only ±0.03 and ±0.05 dex respectively. The sum in quadrature of these uncertainties on the atmospheric parameters gives uncertainties on the abundances of ∼0.12 dex.

Finally, the LTE assumption might not be appropriate for supergiant, variable stars. The adopted stellar atmosphere models could then lead to systematic errors. However, the use of relatively weak lines should minimize this effect. Moreover, Fry & Carney (1997) have shown that a canonical spectroscopic analysis, using LTE atmosphere models, gives reliable abundances for Cepheids: dwarfs and Cepheids located in the same open clusters are found to have the same metallicity, within the errors. Yong et al. (2006) also tested the influence of NLTE effects and showed that the surface gravities derived from a classical approach are robust.

2.8. Distances

Individual Cepheid distances were estimated using near-infrared (J, H, K-band) photometry either collected from SAAO or from the 2MASS catalog. The mean magnitude of the Cepheids based on 2MASS photometry was estimated using the template light curves provided by Soszýnski et al. (2005) together with the V-band amplitude and the epoch of maximum available in the literature. The data from Barnes et al. (1997) were also used for ST Tau and AD Gem while for HW Pup, the data from Schechter et al. (1992) were used together with 2MASS data. In the case of UY Mon and AO CMa that are first overtone pulsators, it is not possible to use the empirical template, since it is only available for fundamental mode pulsators. The mean near-infrared magnitude of these objects is only based on the 2MASS measurement. Their period was fundamentalized as explained below. Note that the SAAO magnitudes were transformed into the 2MASS photometric system using the transformations provided by Koen et al. (2007).

We adopted the individual Cepheid reddenings provided either by Laney & Caldwell (2007) or listed in the Fernie database (Fernie et al. 1995). These two sets of reddenings are not homogeneous, as recent results provided by Laney & Caldwell (2007) are corrected for metallicity effects whereas reddenings from Fernie et al. (1995) do not take into account metallicity effects. The relative absorption in the V-band was estimated using $A_V = 3.1E(B-V)$ with $A_J = 0.28\ A_V$, $A_H = 0.19\ A_V$, and $A_K = 0.11\ A_V$ (Cardelli et al. 1989).

The Cepheid distances were estimated using the near-infrared Period-Luminosity (PL) relations provided by Persson et al. (2004) and by assuming an LMC distance modulus of 18.50, a conservative value adopted by the HST Key Project (Freedman et al. 2001). For a discussion on the LMC distance modulus, please see Romaniello et al. (2008) and references therein. Note that the quoted PL relations were also transformed into the 2MASS photometric system using the transformations provided by Carpenter (2001). In order to estimate the distance of first overtone Cepheids their periods were fundamentalized, i.e. we added 0.127 to their logarithmic period.

Using these PL relations from Persson et al. (2004) for Galactic Cepheids is justified although they are based on a large and homogeneous sample of LMC Cepheids. Current empirical and theoretical findings indicate that the slope and the zero-point of NIR PL relations are not strongly dependent on metallicity (Bono et al. 1999; Persson et al. 2004; Fouqué et al. 2007; Romaniello et al. 2008). Moreover, the near-infrared PL relations present an intrinsic dispersion that is significantly smaller than the dispersion of the optical PL relations. The difference is due to the fact that the former ones are, at fixed period, marginally affected by the intrinsic width in temperature of the instability strip. Finally, Cepheid distances based on near-infrared PL relations are more accurate than optical ones because they are much less affected by uncertainties in reddening estimates.

The heliocentric distance of the stars adopted in the following is the mean value between the three distances in J, H, and K bands to limit random errors. The Galactocentric distance is calculated with the classical formula assuming a Galactocentric distance of 8.5 kpc for the sun (Feast & Whitelock 1997), in order to enable comparisons with Paper I. This determination

Table 3. Cepheid distances.

Object	Galactocentric distance (V) kpc	Galactocentric distance (IR) kpc	Heliocentric distance (IR) kpc
AO Aur	12.60	12.43	3.940
AX Aur	12.79	12.75	4.256
BK Aur	10.72	10.86	2.500
SY Aur	10.71	10.92	2.486
Y Aur	10.27	10.42	1.969
YZ Aur	13.30	12.71	4.278
AO CMa	11.32	11.10	4.068
AA Gem	12.39	12.31	3.820
AD Gem	11.20	11.37	2.939
RZ Gem	10.57	10.66	2.158
BE Mon	10.02	10.11	1.742
BV Mon	10.89	11.19	2.986
CV Mon	10.22	10.09	1.774
EK Mon	10.84	10.71	2.575
SV Mon	10.94	10.82	2.514
TW Mon	14.47	14.00	6.079
TX Mon	12.56	12.34	4.344
TY Mon	11.90	11.94	3.890
TZ Mon	12.22	12.01	3.982
UY Mon	10.74	10.37	2.038
V495 Mon	12.79	12.65	4.679
V508 Mon	11.38	11.43	3.222
V510 Mon	13.73	13.38	5.337
WW Mon	13.68	13.52	5.274
XX Mon	12.68	12.55	4.617
CS Ori	12.42	12.56	4.214
GQ Ori	10.91	10.83	2.469
RS Ori	10.00	10.02	1.575
HW Pup	13.28	13.77	7.795
AV Tau	11.51	11.54	3.043
ST Tau	9.50	9.52	1.044
DD Vel	–	10.69	6.710
EZ Vel	–	12.20	9.522

1st Col.: galactocentric distance from V band photometry; 2nd Col: galactocentric distance from IR photometry; 3rd Col.: Heliocentric distance from IR photometry.

(whose error bars are ±0.5 kpc) was based on the analysis of the Hipparcos proper motion of 220 Cepheids. Recent studies give Galactocentric distances for the sun between 7.62 ± 0.32 kpc (Eisenhauer et al. 2005) and 8.8 ± 0.3 kpc (Collinge et al. 2006). For a recent review of the distance to the Galactic Center, see Groenewegen et al. (2008).

The distances based on near-infrared photometry are given in the second column of Table 3. Galactocentric distances based on V-band photometry for which we adopted the heliocentric distances given in the Fernie database are given *only as a guideline* in the first column (see Fernie et al. 1995, for details). Indeed these distances were estimated using a V-band period-luminosity relation but this relation is not corrected for metallicity effects and was derived using individual reddenings determined from a period-colour relation which doesn't account for the metallicity, whereas these period-colour relations are likely to be metallicity-dependent (Laney & Stobie 1994; Bono et al. 1999).

As expected, the two different sets of distance determinations agree quite well near the solar circle, where the metallicities are in general near to the solar value. However, for lower metallicity objects located in the outer disk, the discrepancy increases and reaches respectively 2.8%, 3.5%, 3.4% and 4.8% in the case of V510 Mon, TW Mon, HW Pup and YZ Aur, 4 stars among the 5 more distant Cepheids in our sample.

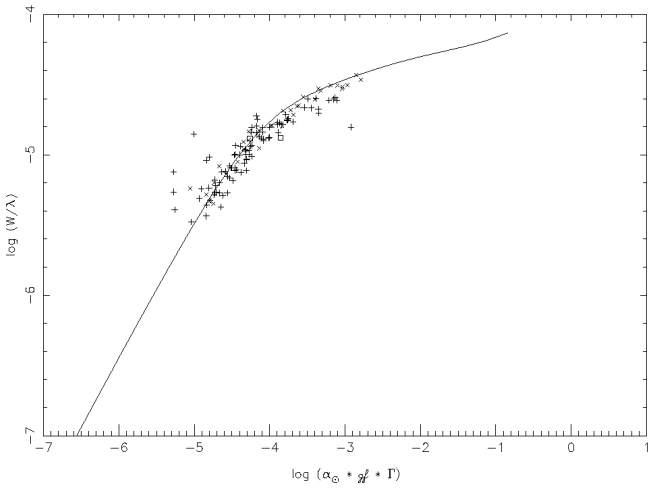

Fig. 1. Observed curve of growth for Fe I in RZ Gem. The full line is the theoretical curve of growth for a typical line (λ = 5000 Å, χ_{ex} = 3). The atmospheric parameters adopted for this star are T_{eff} = 5500 K, $\log g$ = 0.8, v_t = 3.3 km s^{-1}, and [Fe/H] = −0.44 dex. Squares represent lines with χ_{ex} < 1.5 crosses lines with 1.5 < χ_{ex} < 3.0 and pluses lines with χ_{ex} > 3.0.

3. Results: iron abundances

A large fraction of Cepheids in our sample present slightly sub-solar iron abundances, i.e. the metal content expected for Cepheids located in the outer disk. Current results are in very good agreement with previous studies, mainly the series of papers from Andrievsky and collaborators (Andrievsky et al. 2002a,b,c; Luck et al. 2003; Andrievsky et al. 2004, 2005; Kovtyukh et al. 2005a,b; Luck et al. 2006). Indeed 17 stars present small (<0.1 dex) differences in iron abundances. On the other hand, for six stars the differences are ∼0.1 dex and only for four stars (UY Mon, BK Aur, RZ Gem and AO Aur) is the difference higher and approaches 0.3 dex.

The differences could arise from the methods employed to determine abundances, as Andrievsky and collaborators used a modified version of the standard spectroscopic analysis in order to avoid a possible dependence of Fe I lines on NLTE effects, as explained in Kovtyukh & Andrievsky (1999). In their method, surface gravities and microturbulent velocities are derived from Fe II lines instead of Fe I lines. However, the differences are not correlated with specific phases, atmospheric parameters or metallicities. Another difference between the studies is the value of atomic parameters, as Kovtyukh & Andrievsky (1999) derived their $\log g$ through an inverted analysis of the solar spectrum. However, $\log g$ for Fe I are very similar for lines in common. Our list of Fe II lines is about twice as large due to the wider spectral range, and there are only mild differencies for lines in common, except for 2 lines where they reach ≈0.2 dex. Thus differences in atomic parameters cannot be the origin of the discrepancies in iron abundances.

The curves of growth for Fe I (Fig. 1) and for Fe II (Fig. 2) are presented below in the case of RZ Gem. The good agreement between predicted curves of growth and measurements for both Fe I and Fe II as well as the test performed on EWs measurements (see Sect. 2.3) indicate that our abundances measurements are robust. The same outcome applies for the other discrepant Cepheids. However, these stars deserve further investigation as they are all located in the outer disk, which is less well sampled than the solar neighborhood.

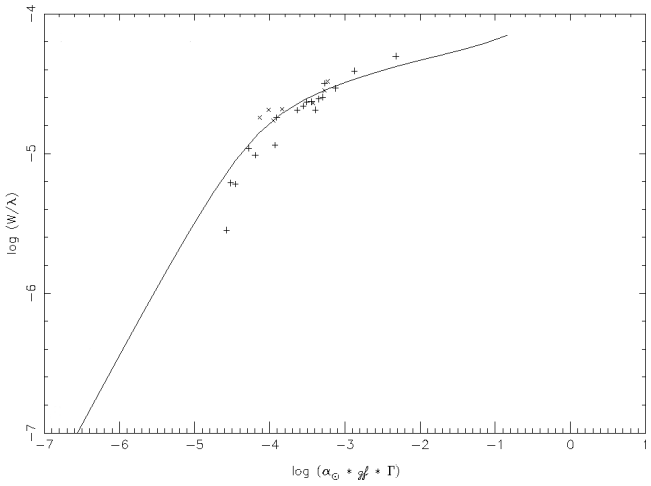

Fig. 2. Same as Fig. 1 but for Fe II.

A few stars have been investigated in many studies and the results are quite often homogeneous (see e.g. SV Mon). Only three stars of our sample (YZ Aur, WW Mon and HW Pup) are in common with both Andrievsky's series and Yong et al. (2006). Although our classical approach is very similar to the analysis performed by Yong et al. (2006), current iron abundances agree quite well with those published in Luck et al. (2006). We found metal abundances that are higher than the values provided by Yong et al. (2006).

This difference cannot be explained by the different approaches adopted in the two investigations to estimate the effective temperature. Indeed, independent support of current $T_{\rm eff}$ values is provided by the evidence that both high and low $\chi_{\rm ex}$ lines properly fit the curve of growth. Moreover, we found that the two investigations adopted different gf-values for the Fe II lines, but the difference is on average smaller than 0.1 dex and the ensuing difference in the estimated surface gravities is negligible. Therefore, this cannot account for the differences in iron abundances. Although our spectra have higher spectral resolution (48 000–81 000 versus 28 000) and higher *S/N* ratio (145, 104, 93 versus 49, 60, 49) than the spectra fromYong et al. (2006), the discrepancies correlate neither with the *S/N* ratio nor with the atmospheric parameters. We cannot reach any firm conclusion regarding this discrepancy, since there are only three objects in common in the two Cepheid samples.

4. Results: galactic abundance gradients

4.1. The iron gradient along the whole Galactic disk

The current sample includes 33 Cepheids and we added to this new data the 30 Cepheids of our previous investigation (Lemasle et al. 2007). The 63 stars of this sample are located between 8 and 15 kpc from the Galactic center (see Fig. 3). We investigated at first the working hypothesis of a linear gradient and calculated the iron Galactic gradient using the entire Cepheid sample. We found a slope of –0.023 ± 0.007 dex kpc^{-1} that is shallower than previous studies. However, this low value can be easily explained by the lack of targets inside the Solar circle: in this region, the metallicities are higher and indeed, inner Cepheids approach abundances of the order of +0.3 dex (Andrievsky et al. 2002b). The inclusion of these Cepheids will then dramatically change the slope of the gradient. Moreover and even more importantly, data plotted in Fig. 3 do not show evidence of a gap over the Galactocentric distances covered by the current Cepheid sample.

Table 4. Cepheid iron abundance and comparisons with previous results.

Object	[Fe/H] dex	[Fe/H]: Previous results dex
AO Aur	–0.41	–0.14[4]
AX Aur	–0.22	
BK Aur	–0.10	0.17[5]
	–0.04	
SY Aur	–0.07	–0.02[8]
Y Aur	–0.26	–0.23[5]
YZ Aur	–0.33	–0.07[1], –0.37[5], –0.64[6], –0.36[8]
AO CMa	–0.04	–0.02[9]
AA Gem	–0.35	–0.24[4]
AD Gem	–0.19	–0.19[4]
RZ Gem	–0.44	–0.12[4]
BE Mon	–0.07	
BV Mon	–0.10	
CV Mon	–0.10	–0.03[1]
EK Mon	–0.05	–0.1[2]
SV Mon	–0.10	–0.03[1], 0.00[2], –0.04[8], –0.02[7]
TW Mon	–0.15	–0.24[3], –0.20[9]
TX Mon	–0.12	–0.14[2]
TY Mon	–0.15	
TZ Mon	–0.04	–0.03[2], –0.12[3], –0.24[9]
UY Mon	–0.33	–0.08[4]
V495 Mon	–0.17	–0.26[2], –0.16[9]
V508 Mon	–0.25	–0.25[2]
V510 Mon	–0.12	–0.19[3], –0.20[6]
WW Mon	–0.32	–0.29[3], –0.25[9], –0.59[6]
XX Mon	–0.18	–0.18[2], –0.08[3]
CS Ori	–0.19	–0.26[2]
GQ Ori	0.11	–0.03[1], 0.06[5]
RS Ori	–0.14	–0.1[1],–0.02[3]
HW Pup	–0.28	–0.29[2], –0.2[3], –0.40[6]
AV Tau	–0.17	
ST Tau	–0.14	–0.05[1]
DD Vel	–0.35	
EZ Vel	–0.01	

[1] Andrievsky et al. (2002a), [2] Andrievsky et al. (2002c), [3] Luck et al. (2003), [4] Andrievsky et al. (2004), [5] Luck et al. (2006), [6] Yong et al. (2006), [7] Kovtyukh et al. (2005a), [8] Kovtyukh et al. (2005b), [9] Pont (1997).

In order to improve the sampling across the Galactic disk, we added to these 63 Cepheids 115 stars from Andrievsky's sample and 10 stars from Romaniello et al. (2008). For the entire Cepheid sample, we have both metallicities and infrared photometry. Among them, 38 Cepheids have Galactocentric distances between 10 and 12 kpc and 27 are even more distant. Individual distances and iron abundances are listed in Table 5. A map (as seen from above the Galaxy) showing the spatial distribution of the Cepheids is displayed in Fig. 4. The x-axis contains both the center of the Galaxy at (0, 0) and the Sun at (8.5, 0). Galactocentric circles with radii of 2 to 18 kpc are overplotted on the map.

By adopting the entire sample we calculated once again the iron Galactic gradient. Note that the new sample includes 60 Cepheids located inside the Solar circle together with two Cepheids located beyond 16 kpc. We found that the slope of the linear iron gradient over the whole sample is –0.052 ± 0.003 dex kpc^{-1} (Fig. 5). This slope is slightly shallower than in Paper I where we found

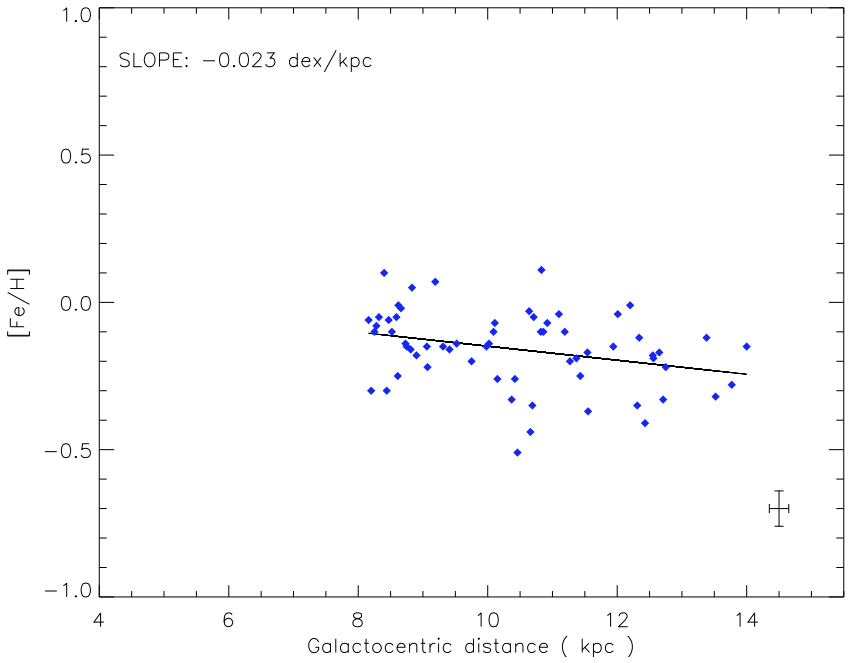

Fig. 3. Galactic iron abundance gradient. The solid line shows the linear regression over the entire sample. Characteristic error bars are plotted in the lower right corner.

Table 5. Additional stars from Andrievsky's series and from Romaniello et al. (2008). The latter are marked with an (*). Distances are based on infrared photometry and [Fe/H] found in the literature.

Object	d_{IR} kpc	[Fe/H] dex	Object	d_{IR} kpc	[Fe/H] dex	Object	d_{IR} kpc	[Fe/H] dex	Object	d_{IR} kpc	[Fe/H] dex	Object	d_{IR} kpc	[Fe/H] dex
TT Aql	7.70	0.11	BD Cas	9.85	–0.07	MW Cyg	8.15	0.09	S Nor	7.74	0.05	RY Sco	7.16	0.09
FM Aql	7.86	0.08	CF Cas	10.30	–0.01	V386 Cyg	8.48	0.11	V340 Nor	6.90	0.00	KQ Sco	6.26	0.16
FN Aql	7.41	–0.02	CH Cas	9.98	0.17	V402 Cyg	8.18	0.02	Y Oph	7.94	0.05	V500 Sco	7.08	–0.02
V496 Aql	7.63	0.05	CY Cas	10.48	0.06	V532 Cyg	8.55	–0.04	BF Oph	7.69	0.00	SS Sct	7.61	0.06
V1162 Aql	7.48	0.01	DD Cas	10.22	0.10	V924 Cyg	7.92	–0.09	SV Per	10.82	0.01	UZ Sct	5.69	0.33
Eta Aql	8.30	0.05	DF Cas	10.45	0.13	V1334 Cyg	8.46	–0.04	UX Per	12.30	–0.21	EW Sct	8.14	0.04
V340 Ara	5.00	0.31	DL Cas	9.46	–0.01	V1726 Cyg	8.73	–0.02	VX Per	10.46	–0.05	V367 Sct	6.81	–0.01
RT Aur	8.93	0.06	FM Cas	9.58	–0.09	Beta Dor	8.50	–0.01	AS Per	9.79	0.10	BQ Ser	7.70	–0.04
RX Aur	10.03	–0.07	V636 Cas	8.96	0.06	W Gem	9.44	–0.04	AW Per	9.29	0.01	SZ Tau	8.94	0.08
AN Aur	11.69	–0.16	V Cen	7.99	0.04	Zeta Gem	8.86	0.04	BM Per	11.30	0.10	AE Tau	12.33	–0.19
CY Aur	13.58	–0.40	CP Cep	9.79	–0.01	V Lac	9.17	0.00	HQ Per	13.95	–0.31	S Vul	7.60	–0.02
ER Aur	16.69	–0.34	CR Cep	9.00	–0.06	X Lac	9.01	–0.02	V440 Per	9.13	–0.05	T Vul	8.35	0.01
RW Cam	10.01	0.04	IR Cep	8.65	0.11	Y Lac	9.08	–0.09	X Pup	10.50	–0.03	U Vul	8.16	0.05
RX Cam	9.25	0.03	Del Cep	8.57	0.06	Z Lac	9.20	0.01	S Sge	8.13	0.10	X Vul	8.10	0.08
TV Cam	12.38	–0.08	BG Cru	8.30	–0.02	RR Lac	9.21	0.13	U Sgr	7.89	0.04	SV Vul	7.80	0.03
AB Cam	12.72	–0.09	X Cyg	8.32	0.12	BG Lac	8.77	–0.01	W Sgr	8.08	–0.01	U Car	8.11	0.12*
AD Cam	13.47	–0.22	SU Cyg	8.17	0.00	V473 Lyr	8.33	–0.06	Y Sgr	8.02	0.06	WZ Car	8.14	0.18*
RW Cas	10.39	0.22	SZ Cyg	8.60	0.09	T Mon	9.75	0.22	VY Sgr	6.29	0.26	VW Cen	6.83	0.05*
RY Cas	9.91	0.26	TX Cyg	8.46	0.20	AA Mon	12.03	–0.21	WZ Sgr	6.71	0.17	XX Cen	7.52	0.04*
SU Cas	8.71	–0.01	VX Cyg	8.58	0.09	CU Mon	14.73	–0.26	XX Sgr	7.18	0.10	KN Cen	6.92	0.07*
SW Cas	9.34	0.13	VY Cyg	8.49	0.00	EE Mon	16.06	–0.51	AP Sgr	7.68	0.10	GH Lup	7.56	0.03*
SY Cas	9.66	0.04	VZ Cyg	8.75	0.05	FG Mon	14.43	–0.20	AV Sgr	6.37	0.34	S Mus	8.12	0.18*
SZ Cas	10.25	0.04	BZ Cyg	8.54	0.19	FI Mon	13.12	–0.18	BB Sgr	7.71	0.08	UU Mus	7.60	0.05*
TU Cas	8.95	0.03	CD Cyg	8.05	0.07	V504 Mon	11.59	–0.31	V350 Sgr	7.62	0.18	U Nor	7.34	0.10*
XY Cas	9.73	0.03	DT Cyg	8.42	0.11	V526 Mon	9.69	–0.13	RV Sco	7.74	0.10	LS Pup	11.39	–0.11*

–0.061 ± 0.019 dex kpc^{-1}, as well as in Friel et al. (2002) who found –0.06 ± 0.01 dex kpc^{-1} from open clusters and in Luck et al. (2006) who found –0.068 ± 0.003 dex kpc^{-1} from classical Cepheids. Data plotted in this figure indicate that:

- the spread in metallicity is larger in the outer disk, in particular around 10 kpc;
- there is no evidence of a gap in the Galactocentric distances covered by the current sample. We will discuss this point in the next section.

4.2. The iron gradient in the outer disk

To properly investigate the iron gradient in the outer disk, we selected (in our sample of 63 stars) Cepheids located between 10 and 15 kpc (see Fig. 6). We estimated the Galactic gradient and found a slope of –0.012 ± 0.014 dex kpc^{-1}. The shallow slope clearly indicates a flattening of the iron gradient in the outer disk. This also suggests that the Galactic iron gradient might be more accurately described by a bimodal distribution. This evidence

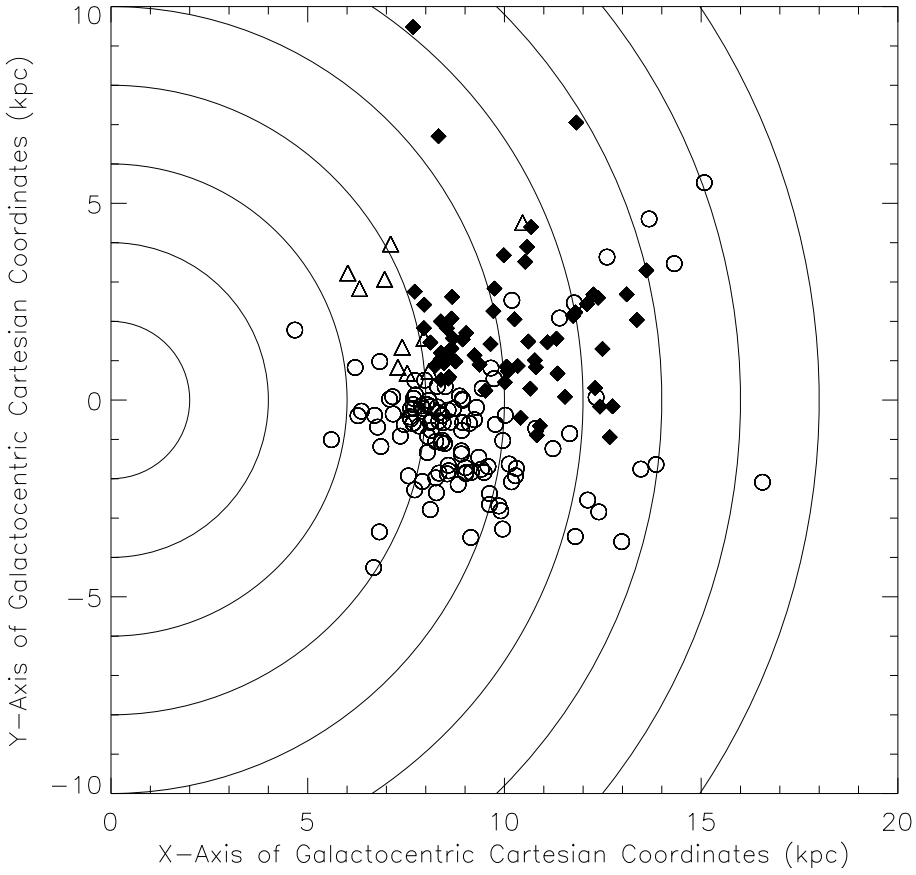

Fig. 4. Spatial distribution of the entire Cepheid sample. Filled diamonds mark our data, while open circles show data from Andrievsky et al. and open triangles are data from Mottini et al. The *x*-axis contains both the center of the Galaxy at (0, 0) and the Sun at (8.5, 0). Galactocentric circles with radii of 2 to 18 kpc are overplotted on the map.

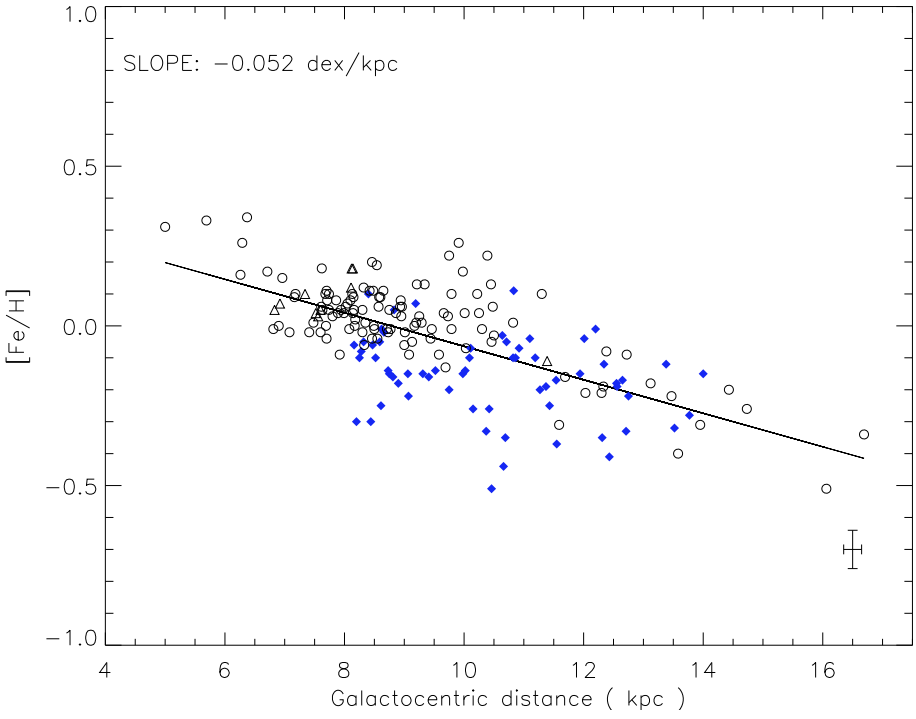

Fig. 5. Galactic iron abundance gradient. Filled diamonds mark our data, open circles show data from Andrievsky et al. and open triangles data from Mottini et al. The solid line shows the linear regression over the entire sample. Characteristic error bars are plotted in the lower right corner.

agrees quite well with the slope (–0.018 ± 0.02 dex kpc^{-1}) recently found by Carraro et al. (2007) using old Open Clusters ranging from 12 to 21 kpc and a Galactocentric distance of the Sun of 8.5 kpc. It is also similar to the flat distribution (+0.004 ± 0.011) found by Andrievsky et al. (2004) in the outer zone (zone III) of their multimodal gradient. Moreover and even more importantly, the two quoted independent investigations suggest, within the errors, a similar result concerning the value of the metallicity basement. The value of the metallicity basement we found from our data is –0.19 ± 0.14 dex, whereas Carraro et al. (2007) found that open clusters located in the outer disk have an iron abundance of [Fe/H] = 0.34 ± 0.15 dex, a value close to the ∼–0.3 dex found by Twarog et al. (1997) from the same kind of objects. Our basement value also

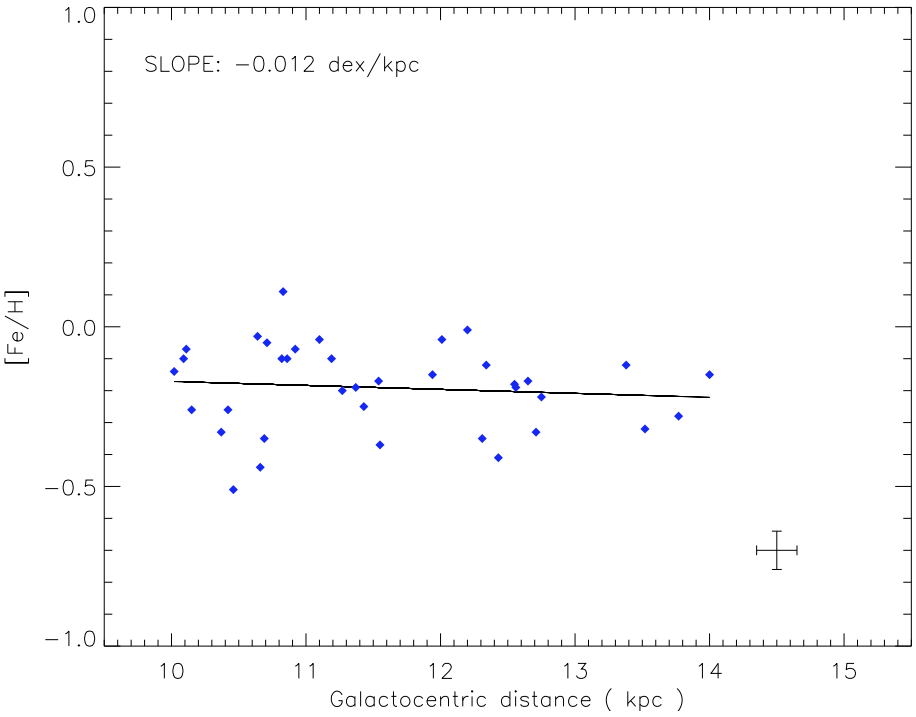

Fig. 6. Same as Fig. 3, but for Cepheids with Galactocentric distances ranging from 10 to 15 kpc.

agrees very well with the one of Andrievsky et al. (2004) as the mean iron abundance obtained in their outer disk zone is –0.209 ± 0.058 dex.

Current findings are marginally consistent with the results concerning the metallicity basement by Yong et al. (2006). They suggested a two-level basement in the outer disk: one level located at ∼–0.5 dex, is notably lower than the other values, while the second one is still lower at ∼–0.8 dex. According to these authors, the more metal-poor values might be explained by Cepheids acquired by the Galaxy through merging events. This working hypothesis was also supported by the significantly different [α/Fe] ratios shown by these objects. In this context, Yong et al. (2005) and Carney et al. (2005) using different stellar tracers, namely open clusters and field red giants, found a metallicity basement of ≈–0.5 dex.

If we now study the same region including all the Cepheids for which we have accurate estimates of both iron abundance and distance, the gradient is affected by selection effects. The value of the slope depends on:

- the range of Galactocentric distances covered by the Cepheid sample, since the targets are not uniformly distributed along the disk;
- the spatial sampling across the disk. By using Cepheids in our sample with $R \geq 10$ kpc we found a slope of -0.012 ± 0.014 dex kpc^{-1}. On the other hand, if we use Cepheids from the Andrievsky sample and our distances we found a slope of -0.077 ± 0.010 dex kpc^{-1}, while with two samples together we obtain a slope of -0.050 ± 0.008 dex kpc^{-1} (see Fig. 7).

The quoted results are strongly affected by the poor spatial sampling. The number of known Cepheids located in the outer disk is quite limited and quite often they are also relatively faint. This means that long exposure times with 4–8 m class telescopes are necessary to obtain the *S/N* required for accurate spectroscopy.

The other interesting findings brought forward by the data plotted in Fig. 7 is the large spread in metallicity between 10 and 12 kpc. This feature was partially expected and is caused by the decrease in gas density and in star formation rate when moving from the innermost to the outermost regions of the Galaxy.

- A group of Cepheids has rather high metallicities (∼+0.0 to ∼+0.2 dex). Some of them were already noted by Luck et al. (2006) to be located approximately at the same Galactic longitude ∼120°.
- On the contrary, a group of stars has rather low metallicities (∼–0.2 to ∼–0.4 dex), most of them lying in the $180° < l < 200°$ range of Galactic longitudes.

According to this circumstantial empirical evidence, if we plot the Cepheids located between 10 and 12 kpc on a Galactocentric polar map (see Fig. 8), we can see that the metallicity is dependent on the Galactocentric longitude, with a spread in metallicity reaching 0.8 dex for stars located at roughly the same Galactocentric distance. Here we define the Galactocentric longitude as the angle of a polar coordinate system centered on the Galactic center. Galactocentric longitudes are measured from –180° to +180°, counter clockwise from the origin, arbitrarily defined as the Galactic radius containing the Galactic center at (0, 0) and the Sun at (8.5, 0). Distances projected on Galactocentric Cartesian coordinates are also labelled on the x and y-axis.

The occurrence of a large spread in metal abundance between stars located at the same radius of the Galactic disk allows us to explain why we do not observe a gap in the Galactic gradient as proposed in some previous studies. The gap might be caused either by selection effects in the sampling of the disk, or by local inhomogeneities in the disk, and therefore, restricted to a narrow range in longitude. The Cepheid sample collected by Andrievsky et al. (2002c), Luck et al. (2003), Andrievsky et al. (2004) are indeed located in a limited range of Galactic longitude ($190° < l < 250°$). The same outcome applies to the sample of 76 Open Clusters collected by Twarog et al. (1997) ($130° < l < 260°$).

Current findings suggest the need to be very cautious in using the slopes of Galactic gradients, in particular in the outer disk due to poor spatial sampling. A significant improvement in

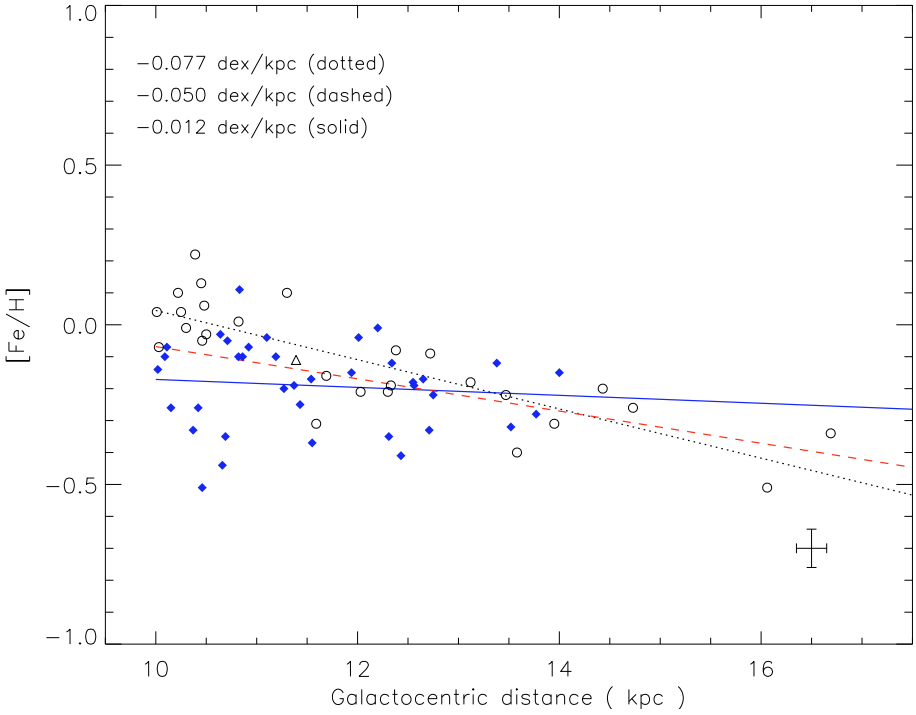

Fig. 7. Galactic iron abundance gradient. Filled diamonds mark our data, while open circles show data from Andrievsky et al. and open triangles display data from Mottini et al. The solid line shows the slope based on our sample, the dotted line the slope based on the additional data from Andrievsky et al. and the dashed line the slope obtained using the two quoted samples. Characteristic error bars are plotted in *the lower right corner*.

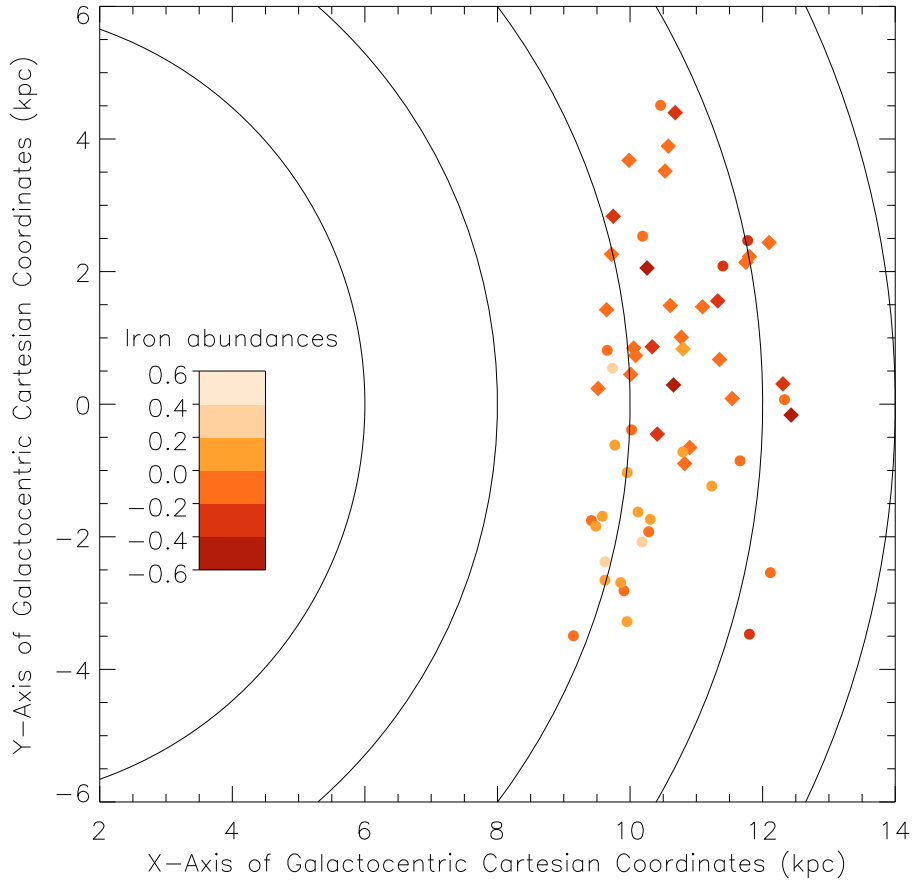

Fig. 8. Metallicity of Cepheids located between 10 and 12 kpc. Filled diamonds mark our data while filled circles show data from Andrievsky et al. The metallicity strongly depends on the Galactocentric longitude (see text). The center of the Galaxy is at (0, 0) and the Sun is at (8.5, 0). Galactocentric circles with radii of respectively at 6, 8, 10, 12 and 14 kpc are overplotted on the map.

the sample of outer disk Cepheids requires a systematic photometric survey to detect new Cepheids. This goal can be achieved with the new generation of automatic telescopes such as HAT (Hungarian-made Automated Telescope; http://cfa-www.harvard.edu/~gbakos/HAT/index.html) or ASAS (All Sky Automated Survey; http://archive.princeton.edu/~asas/) and with spectroscopic follow up of the new targets.

5. Conclusions

High resolution spectra and accurate distance determinations based on infrared photometry allowed us to extend our study of the Galactic iron abundance gradient toward the outer disk. New data led us to a slope of –0.052 ± 0.003 dex kpc^{-1} in the 5–17 kpc range, in very good agreement with previous studies if we consider a linear gradient. However, the Galactic iron

abundance gradient is better described by a bimodal distribution with a steeper slope toward the bulge and a flattening of the gradient toward the outer disk. In particular, we found a shallow slope of -0.012 ± 0.014 dex kpc^{-1} in this region (10–15 kpc). Current data show no evidence of a sharp discontinuity in metallicity for Galactocentric radii of ~10–12 kpc. Poor spatial sampling affecting the adopted stellar tracers do not allow us to constrain on a quantitative basis whether the occurrence of this gap is real or caused by local inhomogeneities in the metallicity distribution of the disk. We also found a large spread in metal abundance (≈0.8 dex) for Cepheids located approximately at the same distance ($10 \leq R \leq 12$ kpc), but covering a broad range of Galactocentric longitude. A larger Cepheid sample, uniformly distributed over the four Galactic quadrants, is mandatory to constrain this effect.

Acknowledgements. This research has made use of the SIMBAD and VIZIER database, operated at CDS, Strasbourg, France. We thank the staff of the CFHT and of the TBL and SciOps at La Silla Observatory for their support during observations. We deeply thank V. V. Kovtyukh for checking our temperatures with his new relations for line depth ratios and S. M. Andrievsky, our referee, for his very useful comments and suggestions.

References

Afflerbach, A., Churchwell, E., & Werner, M. W. 1997, ApJ, 478, 190
Andrievsky, S. M., Kovtyukh, V. V., Luck, R. E., et al. 2002a, A&A, 381, 32
Andrievsky, S. M., Bersier, D., Kovtyukh, V. V., et al. 2002b, A&A, 384, 140
Andrievsky, S. M., Kovtyukh, V. V., Luck, R. E., et al. 2002c, A&A, 392, 491
Andrievsky, S. M., Luck, R. E., Martin, P., & Lépine, J. R. D. 2004, A&A, 413, 159
Andrievsky, S. M., Luck, R. E., & Kovtyukh, V. V. 2005, AJ, 130, 1880
Barnes, T. G., Fernley, J. A., Frueh, M. L., et al. 1997, PASP, 109, 64
Berdnikov, L. N., & Ignatova, V. V. 2000, ASPC 2003, 244
Bono, G., Caputo, F., Castellani, V., & Marconi, M. 1999, ApJ, 512, 711
Cardelli, J. A., Clayton, G. C., & Mathis, J. S. 1989, ApJ, 345, 245
Carney, B. W., Yong, D., & de Almeida, M. L. T. 2005, AJ, 130, 1111
Carpenter, J. M. 2001, AJ, 121, 2851
Carraro, G., Geisler, D., Villanova, S., Frinchaboy, P. M., & Majewski, S. R. 2007, A&A, 476, 217
Cescutti, G., Matteucci, F., François, P., & Chiappini, C. 2007, A&A, 462, 943
Charbonneau, P. 1995, ApJS, 101, 309
Chiappini, C., Matteucci, F., & Romano, D. 2001, ApJ, 554, 1044
Clegg, R. E. S., & Bell, R. A. 1973, MNRAS, 163, 13
Collinge, M. J., Sumi, T., & Fabrycky, D. 2006, ApJ, 651, 197
Costa, R. D. D., Uchida, M. M. M., & Maciel, W. J. 2004, A&A, 423, 199
Daflon, S., & Cunha, K. 2004, ApJ, 617, 1115
Deharveng, L., Pena, M., Caplan, J., & Costero, R. 2000, MNRAS, 311, 329
D'Odorico, S., Peimbert, M., & Sabbadin, F. 1976, A&A, 47, 341
Donati, J.-F., Semel, M., Carter, B. D., Rees, D. E., & Cameron, A. C. 1997, MNRAS, 291, 658
Donati, J.-F., Catala, C., Landstreet, J. D., et al. 2007, MNRAS, in preparation
Edvardsson, B., Andersen, J., Gustafsson, B., et al. 1993, A&A, 275, 101
Eisenhauer, F., Genzel, R., Alexander, T., et al. 2005, ApJ, 628, 246
Feast, M., & Whitelock, P. 1997, MNRAS, 291, 683
Fernie, J. D., Beattie, B., Evans, N. R., & Seager, S. 1995, IBVS N° 4148
Fouqué, P., Arriagada, P., Storm, J., et al. 2007, A&A, 476, 73
Freedman, W. L., Madore, B. F., Gibson, B. K., et al. 2001, ApJ, 553, 47
Friel, E. D., Janes, K. A., Tavarez, M., et al. 2002, AJ, 124, 2693
Fry, A. M., & Carney, B. W. 1997, AJ, 113, 1073
Grevesse, N., Noels, A., & Sauval, J. 1996, ASPC, 99, 117
Groenewegen, M. A. T., Udalski, A., & Bono, G. 2008, A&A, 481, 441
Gummersbach, C. A., Kaufer, D. R., Schäfer, D. R., Szeifert, T., & Wolf, B. 1998, A&A, 338, 881
Harris, H. C. 1981, AJ, 86, 707
Harris, H. C. 1984, ApJ, 282, 655
Janes, K. A. 1979, ApJS, 39, 135
Jennens, P. A., & Helfer, H. L. 1975, MNRAS, 172, 681
Kaufer, A., Stahl, O., Tubbesing, S., et al. 1999, Msngr, 95, 8
Koen, C., Marang, F., Kilkenny, D., & Jacobs, C. 2007, MNRAS, 380, 1433
Kovtyukh, V. V. 2007, MNRAS, 378, 617
Kovtyukh, V. V., & Andrievsky, S. M. 1999, A&A, 351, 597
Kovtyukh, V. V., & Gorlova, N. I. 2000, A&A, 358, 587
Kovtyukh, V. V., Andrievsky, S. M., Belik, S. I., & Luck, R. E. 2005a, AJ, 129, 433
Kovtyukh, V. V., Wallerstein, G., & Andrievsky, S. M. 2005b, PASP, 117, 1173
Laney, C. D., & Stobie, R. S. 1994, MNRAS, 266, 441
Laney, C. D., & Caldwell, J. A. R. 2007, MNRAS, 377, 147
Lemasle, B., François, P., Bono, G., et al. 2007, A&A, 467, 283
Luck, R. E., Gieren, W. P., Andrievsky, S. M., et al. 2003, A&A, 401, 939
Luck, R. E., Kovtyukh, V. V., & Andrievsky, S. M. 2006, AJ, 132, 902
Maciel, W. J., & Quireza, C. 1999, A&A, 345, 629
Romaniello, M., Primas, F., Mottini, M., A&A, 488, 731
Persson, S. E., Madore, B. F., Krzemiński, W., et al. 2004, AJ, 128, 2239
Pont, F., Ph.D. Thesis, Genève
Rolleston, W. R. J., Smartt, S. J., Dufton, P. L., & Ryans, R. S. I. 2000, A&A, 363, 537
Samus, N. N., & Durlevich, O. V. 2004, VizieR On-line Data Catalog: II/250
Schechter, P. L., Avruch, I. M., Caldwell, J. A. R., & Keane, M. J. 1992, AJ, 104, 1930
Searle, L. 1971, ApJ, 168, 327
Soszýnski, I., Gieren, W., & Pietrzýnski, G. 2005, PASP, 117, 823
Stanghellini, L., Guerrero, M. A., Cunha, K., Manchado, A., & Villaver, E. 2006, ApJ, 651, 898
Szabados, L. 1991, Comm. Konkoly Obs., 96, 123
Twarog, B. A., Ashman, K. M., & Antony-Twarog, B. J. 1997, AJ, 114, 2556
Vilchez, J. M., & Esteban, C. 1996, MNRAS, 280, 720
Yong, D., Carney, B. W., & de Almeida, M. L. T. 2005, AJ, 130, 597
Yong, D., Carney, B. W., de Almeida, M. L. T., & Pohl, B. L. 2006, AJ, 131, 2256